

# The Embedded Super Star Cluster of SBS 0335-052<sup>1</sup>

Stéphanie Plante

*Département de physique, de génie physique et d'optique, Université Laval and  
Observatoire du Mont Mégantic, Québec, QC, Canada, G1K 7P4*

splante@phy.ulaval.ca

and

Marc Sauvage

*DAPNIA/Service d'Astrophysique, CEA/Saclay, 91191 Gif-sur-Yvette Cedex, France*

msauvage@cea.fr

## ABSTRACT

We analyze the infrared (6-100  $\mu\text{m}$ ) spectral energy distribution of the blue compact dwarf and metal-poor ( $Z=Z_{\odot}/41$ ) galaxy SBS 0335-052. With the help of DUSTY (Ivezić et al. 1999), a program that solves the radiation transfer equations in a spherical environment, we evaluate that the infrared (IR) emission of SBS 0335-052 is produced by an embedded super-star cluster (SSC) hidden under  $10^5 M_{\odot}$  of dust, causing 30 mag of visual extinction. This implies that one cannot detect any stellar emission from the  $2 \times 10^6 M_{\odot}$  stellar cluster even at near-infrared (NIR) wavelengths. The derived grain size distribution departs markedly from the widely accepted size distribution inferred for dust in our galaxy (the so-called MRN distribution, Mathis et al. (1977)), but resembles what is seen around AGNs, namely an absence of PAH and smaller grains, and grains that grow to larger sizes (around 1  $\mu\text{m}$ ). The fact that a significant amount of dust is present in such a low-metallicity galaxy, hiding from UV and optical view most of the star formation activity in the galaxy, and that the dust size distribution cannot be reproduced by a standard galactic law, should be borne in mind when interpreting the spectrum of primeval galaxies.

*Subject headings:* galaxies: compact, galaxies: dwarf, galaxies: individual: SBS 0335-052, galaxies: starburst

---

<sup>1</sup>This paper is based: (1) on data obtained with ISO, an ESA project with instruments funded by

## 1. Introduction

The question of how the energy radiated by a very young burst of star formation is re-distributed in the electromagnetic spectrum by the neighboring ISM is one with far-reaching implications. Indeed, as it is generally assumed that the formation of galaxies should be signalled by violent bursts of star formation (see e.g. the reviews by Silk & Devriendt (2001) or Ellis (1998), and references therein), the answer to this question can help defining the best observing strategy to study primeval galaxies. For the most massive objects, it is generally assumed that star formation proceeds as observed in Ultra-Luminous InfraRed Galaxies (ULIRGs, see the review by Sanders & Mirabel (1996)). In these systems, we know that most of the energy emerges in the infrared, and this would tend to invalidate any result derived from optical-UV surveys of the distant Universe. Yet studies on the local starburst galaxy population appear to indicate a correlation between the total infrared luminosity and the extinction as measured by the slope of the UV continuum (Meurer et al. 1995). Such a correlation, along with the establishment of an effective attenuation curve (Calzetti et al. 1994), offers the hope to address the question of galaxy formation with optical-UV instruments, thus circumventing an important problem of most current infrared and submillimeter instruments: their lower spatial resolution that makes the identification of counterparts and subsequent determination of redshifts problematic.

However a number of relatively recent discoveries on the properties of starburst galaxies and ULIRGs cast some doubt on the potential of this UV-IR/Submm relation and on the physical meaning of an attenuation curve for getting at the intrinsic UV luminosity of a starburst galaxy. Recent high-spatial resolution MIR instruments have revealed the existence of very bright super star-clusters (clusters containing a few thousand O stars, hereafter SSCs) that are nearly or absolutely absent from visible images, e.g. the deeply buried SSC found in the Antennae galaxy (Mirabel et al. 1998). This object produces about 20% of the total MIR emission of the whole galaxy and was shown by Gilbert et al. (2000) to be a very young ( $\sim 4$  Myr) SSC containing  $1.6 \times 10^7 M_{\odot}$  of stars embedded in an  $A_V = 10$  cloud of dust. This is no longer an isolated case: the Wolf-Rayet dwarf galaxy He2-10 is an even

---

the ESA member states (especially the PI countries: France, Germany, the Netherlands, and the United Kingdom) with the participation of ISAS and NASA, (2) on observations obtained at the Gemini Observatory, which is operated by the Association of Universities for Research in Astronomy, Inc., under a cooperative agreement with the NSF on behalf of the Gemini partnership: the National Science Foundation (United States), the Particle Physics and Astronomy Research Council (United Kingdom), the National Research Council (Canada), CONICYT (Chile), the Australian Research Council (Australia), CNPq (Brazil) and CONICET (Argentina), using the mid-infrared camera OSCIR, developed by the University of Florida with support from the National Aeronautics and Space Administration, and operated jointly by Gemini and the University of Florida Infrared Astrophysics Group.

more impressive example of the buried SSC phenomenology. Kobulnicky & Johnson (1999) showed that He2-10 contains extremely compact radio sources whose spectrum is optically thick at 5 GHz, which are interpreted as ultra-dense HII regions created by dust-embedded SSCs each with  $\sim 750$  O7V stars. Gemini/OSCIR high resolution MIR observations by Vacca et al. (2002) showed that the radio SSCs are exactly coincident with the MIR emitting regions observed previously by Sauvage et al. (1997); the SSCs generate *almost all* of the MIR luminosity of the galaxy, and there is *no overlap* between the MIR emitting regions and those detected in the K band. This is also true with the L and M bands (Sauvage et al. 2002) implying a very high optical depth along the line of sight toward the SSCs. Another case where the infrared emission arises from a dust-embedded SSC with no optical counterpart is the dwarf galaxy NGC 5253 (Turner et al. 2000; Gorjian et al. 2001).

Recent observations have shown that dust is present even in the most metal-deficient objects in amounts large enough to affect our ability to observe the star-formation process, namely IZw 18 and SBS 0335-052. In IZw 18, still the most metal-poor galaxy known at  $Z=Z_{\odot}/50$ , the analysis of the  $H\alpha/H\beta$  ratio by Cannon et al. (2002) indicates patches of dust inside the HII regions that lead to  $A_V = 0.5$  mag in some places.

SBS 0335-052, at  $Z_{\odot}/41$ , for which we are presenting new data, has the highest star formation rate of the two. Thuan et al. (1997), based on HST images, argue that this galaxy is probably undergoing its first burst of star formation (but see Östlin & Kunth (2001), and consider that the aim of this paper is *not* to discuss whether or not SBS 0335-052 undergoes its first burst of star formation, but rather to show that the *current* burst properties can shed light on phenomena possibly occurring in primeval galaxies. In other words, SBS 0335-052 is considered in this work as a laboratory to study primeval galaxies, but not as a primeval galaxy itself). In HST images, young stars appears concentrated in 6 SSCs, each of them not older than 25 Myr and all located within a region smaller than  $526 \text{ pc}^2$ . In the NIR, the emission originates mostly from a region coincident with two of these SSCs (the ground-based NIR image does not allow to precisely attribute the emission to the HST-detected SSCs). The NIR spectrum indicates stellar populations younger than 5 Myr (Vanzi et al. 2000). The picture gets more complex when the MIR properties are considered as well: the galaxy is very bright in the MIR and its global MIR spectrum is quite unusual (Thuan et al. (1999b), hereafter Paper I). First, it is lacking the Unidentified Infrared Bands (UIB) commonly attributed to Polycyclic Aromatic Hydrocarbons or PAHs, (Léger & Puget 1984; Allamandola et al. 1985). This is generally indicative of dust exposed to a strong radiation field that either destroys the UIB carriers or swamps their emission in that of the very

---

<sup>2</sup>With  $H_0 = 75 \text{ km s}^{-1} \text{ Mpc}^{-1}$ . At this distance,  $1''$  is  $263 \text{ pc}$ .

small grains. Second it shows a marked silicate absorption band at  $9.7\ \mu\text{m}$ , very unusual at the galaxy scale and indicative of a large dust column density, unexpected in such a low metallicity galaxy. This peculiar spectrum led to the hypothesis that the MIR emission originates from a dust-enshrouded SSC. Subsequent ground-based observations by Dale et al. (2001) showed the MIR emission to be almost a point source coincident with the NIR emitting region; Contrary to Paper I, these authors argued against the buried SSC case for SBS 0335-052. Thus whether SBS 0335-052 contains one or more deeply buried SSCs remains an open question (many different  $A_V$  have been determined for the SSCs of SBS 0335-052, ranging from  $A_V \sim 0.55$  based on the Balmer decrement (Izotov et al. 1997) to  $A_V \sim 20.0$  based on MIR spectroscopy, Paper I), and is worth returning to.

In section §2 we present new GEMINI/OSCIR and ISOPHOT observations used in conjunction with the ISOCAM data to reconstruct the infrared spectral energy distribution of the galaxy. In section §3 we define and justify our assumptions regarding the modelling of radiation transfer in SBS 0335-052. Our results are presented in section §4, and their implications are discussed in section §5.

## 2. Observations

The data used to model the infrared spectral energy distribution of SBS 0335-052 come from three sources. The MIR ISOCAM data were presented in Paper I. The ISOPHOT 60-100  $\mu\text{m}$  data were obtained in the same program as Paper I but their analysis deferred until a full modelling of the SED was possible. The GEMINI MIR data were obtained as a follow-up to clarify the issues developed in Paper I.

### 2.1. ISOPHOT observations

The ISOPHOT (Lemke et al. 1996) data were obtained on revolution 845, using the observation template PHT22, which consists in a small raster around the target. SBS 0335-052 was observed with the C100 detector, in three relatively broad-band filters, namely the 50  $\mu\text{m}$  filter ( $\lambda_{ref} = 65\ \mu\text{m}$ ,  $\Delta\lambda = 57.8\ \mu\text{m}$ ), the 60  $\mu\text{m}$  filter ( $\lambda_{ref} = 60\ \mu\text{m}$ ,  $\Delta\lambda = 23.9\ \mu\text{m}$ ), and the 100  $\mu\text{m}$  filter ( $\lambda_{ref} = 100\ \mu\text{m}$ ,  $\Delta\lambda = 43.6\ \mu\text{m}$ ). As some confusion may arise regarding the relative positioning of the 50 and 60  $\mu\text{m}$  filters, we refer to the ISOPHOT filters by their reference wavelengths, i.e. 60, 65 and 100  $\mu\text{m}$ . The definition of ISOPHOT bandpasses and spectral conventions can be found in Laureijs et al. (2000a), and have been used in this paper when comparing our model SED to the observations. All three data sets were acquired in a

similar fashion, with the  $3\times 3$  pixel C100 detector performing a  $3\times 3$  raster around the source position. The raster axes were aligned with that of the detector and the step between each of the raster point was equal to the pixel size ( $43''.5$ ) so that each pixel sees the center of the field once during the observation (or equivalently, the center of the field is observed by all nine pixels). Operation of the C100 detector consists in a series of non-destructive readouts for a given integration time, called integration ramps, after which a destructive readout resets the detector and a new ramp starts. For all three rasters, the individual integration ramps consisted in 64 readouts. Each ramp lasted 2s. For the 60 and 100  $\mu\text{m}$  filters we took 32 integration ramps per raster position, while this was doubled to 64 ramps for the 65  $\mu\text{m}$  filter.

To analyze the data, we combined the standard PHT reduction steps with a series of algorithms designed to take into account the fact that the source is extremely faint, and very likely point-like (it is not resolved by ISOCAM, and barely by 8 m telescopes on the ground, see later and Dale et al. (2001)). The standard data reduction steps were performed with PIA 7.0<sup>3</sup>. We will not detail here the entire process but rather show at which points we have branched personally developed algorithms. At the ramp stage, we found that the deglitching methods available in PIA 7.0 were not as robust and discriminating as was necessary, and we used instead an adaptation of the multi-resolution deglitching method designed for ISOCAM data (Starck et al. 1999). At this stage a very small percentage ( $\leq 1\%$ ) of the readouts is discarded because glitches typically appear to affect only one of the 64 readouts per ramp. However, once we computed the ramp slopes, we found that the slope signal showed a large number of positive spikes, extremely reminiscent of glitches, affecting up to three consecutive ramps. Inspecting the list of discarded readouts at the ramp stage, we found that *all* the slope spikes could be tied to a glitch impact affecting a readout in the corresponding ramp or the one just preceding (although not all glitches at the readout level lead to a spike in the ramp). This is very similar to glitches with “memory effect” experienced in the CAM LW detector (Starck et al. 1999), and given the similarities in the underlying detector physics, we attribute these spikes to cosmic ray impacts. Since a large number of ramps were obtained per raster position, a multi-resolution method again proved extremely efficient.

Due to the lack of a physical modelling of the transient behavior of the C100 detector, we decided not to apply any transient correction to our data. At the current stage, this would in fact correspond to an arbitrary choice of a correcting function.

---

<sup>3</sup>PIA is a joint development by the ESA Astrophysics Division and the ISOPHOT consortium, with the collaboration of the Infrared Analysis and Processing Center (IPAC) and the Instituto de Astrofísica de Canarias (IAC).

Finally, the last stage of the reduction, the map reconstruction was also replaced by a better suited algorithm. Indeed inspection of the signal from individual pixels revealed that the source only illuminates one pixel of the detector at a given time, i.e. that it is point-like for ISOPHOT. Therefore a simpler method for detecting and measuring the source flux is to use each pixel of the detector as a scanner and co-add these scans (obviously taking into account the fact that the source appears at a different position along each scan). Assuming that the background around the source is constant, we use the off-source sectors of the scan to derive the flat-field of the detector. Finally, the point-spread function profile is used to extract the source flux.

With this processing, the source is clearly detected at  $65\ \mu\text{m}$ . At  $60$  and  $100\ \mu\text{m}$ , the coadded scans do show the expected square signal where the source should be, but the deviation is not statistically significant at the  $3\sigma$  level. Hence we use the  $3\sigma$  upper limits in our analysis. The photometric measurements are compiled in Table 1.

## 2.2. Gemini/OSCIR observations

To constrain the size of the MIR emission from the source and obtain photometric data outside the second silicate absorption band at  $18\ \mu\text{m}$  that was apparent in the ISOCAM spectrum (Paper I), we observed SBS 0335-052 on the night of Dec 9, 2000, at the Gemini-North telescope, with the University of Florida mid-IR camera OSCIR. OSCIR uses a  $128\times 128$  pixel Si:As detector with a plate scale of  $0.089''/\text{pixel}$  providing a field of view of  $11''\times 11''$  on the sky<sup>4</sup>. We used the N-wide filter ( $\lambda_{ref}=10.8\ \mu\text{m}$  and  $\Delta\lambda=4.61\ \mu\text{m}$ ) and the Q3 filter ( $\lambda_{ref}=20.97\ \mu\text{m}$  and  $\Delta\lambda=1.05\ \mu\text{m}$ )<sup>5</sup>. In the rest of this paper, we will refer to these filters as the  $10.8$  and  $21\ \mu\text{m}$  filters.

All the observations were performed using the standard technique of chopping and nodding, with a chop throw of  $15''$  in declination. To obtain the most accurate photometry as possible, we alternatively observed the source and standards at both wavelengths. The standard stars used were  $\beta$  Peg,  $\delta$  Eri, and  $\alpha$  Tau. Flux density estimates for the standard stars were calculated using the SED's published by Cohen et al. (1999). From this, it appeared that although the seeing remained constant during the observations, at  $0''.7$  at  $21\ \mu\text{m}$  and  $0''.43$  at  $10.8\ \mu\text{m}$ , the sky transparency changed during the  $10.8\ \mu\text{m}$  observation of

---

<sup>4</sup>Detailed information on the instrument is available on the web at <http://www.gemini.edu/sciops/instruments/oscir/>

<sup>5</sup>These bandpasses are computed assuming a  $\lambda f_{\lambda}=\text{ct}$  spectral convention. This convention is thus identical for the ISOCAM, ISOPHOT and Gemini/OSCIR data presented in this paper.

SBS 0335-052, after which it remained stable to within  $\pm 5\%$  for the rest of the observations.

Custom routines were used to stack the data appropriately to extract the source signal, however since the source is faint even for Gemini/OSCIR, no shift-and-add was possible. During our observations the OSCIR detector exhibited excess noise in one of its 16 output channels. The main effect of this problem was an offset one, rather than a gain one. This is very reminiscent of the dark current problem encountered on ISOCAM and, to remove this noise, we applied the same ISOCAM algorithm to the OSCIR data to remove that striping pattern (Starck et al. 1999). On these corrected images, the source is clearly detected at both wavelengths. On the reduced images, the source appeared to be point-like or only slightly more extended than the PSF. Therefore the data were ideally suited for filtering and detection based on a wavelet decomposition of the image (compact source in a large image with little or no background structure). To perform the detection and photometry of the object, we have used the *MR1* package<sup>6</sup>. This is a wavelet-based data reduction toolkit that implements all the methods described in Starck et al. (1998). The principle of the method is to decompose the image in a cube where each plane holds only the structures of a characteristic spatial scale, filter these planes, apply a detection algorithm to identify significant deviations in the planes, and reconstruct the detected objects. In this process we are helped by the fact that the PSF is extremely over-sampled and thus even the smallest significant structures are on a larger scale than most of the noise. This process resulted in a clear detection of the galaxy in both wavelengths with a respective positioning well inside the relative pointing accuracy. To constrain our global photometric accuracy, we have performed simulations of the filtering and detection process. At the level of the source signal, with respect to the noise level, the galaxy is detected in 100% of the simulations. However at such faint levels, the photometric accuracy is poor, i.e. typically 30% at both wavelength. Taking into account the transparency variations during the  $10.8\ \mu\text{m}$  observation, the resulting photometric accuracy for that wavelength is 50% (see Table 1). One should note that with this wavelet processing, it is not possible to define a S/N or a standard deviation that could be tied to the source flux, as the noise is essentially filtered out when we perform the photometric measurement. Only simulations of the detection process can indicate the validity of the source. The uncertainties we quote here therefore concern only the photometric calibration of our data, and not the source detection. Uncertainties attached to the source detection can be estimated from the fraction of the simulations that either do not detect the source or produce a false detection at the same flux level. Our experiments show that this fraction is negligible.

In the resulting images, the source has a morphology similar to that of a point source.

---

<sup>6</sup>See <http://www.multiresolution.com>

We therefore have no evidence for an extended component to the MIR emission. We note however that with a seeing FWHM of  $0''.43$  at  $10.8\ \mu\text{m}$  we are not able to confirm or contradict the conclusion of Dale et al. (2001) that the infrared source has a FWHM of  $0''.31$ .

### 3. Model of the infrared SED

#### 3.1. Choice of a radiation transfer model

The global infrared spectral energy distribution (SED) of SBS 0335-052 is displayed in Figure 1. It now shows a further striking feature with respect to what was presented in Paper I, namely that the SED peaks at  $60\ \mu\text{m}$ , a much shorter wavelength than what is observed in normal galaxies. This places SBS 0335-052 in the category of galaxies called “ $60\ \mu\text{m}$  peakers” in the IRAS language. Galaxies with this type of infrared SED are either compact starburst or Seyfert with relatively high NIR extinction (Heisler & de Robertis 1999). Silicate absorption in the MIR is not uncommon, though it is rather restricted to the Seyfert galaxies (Laureijs et al. 2000b). That the emission peaks at  $60\ \mu\text{m}$  probably indicates that SBS 0335-052 lacks the dust phase that is most common in other galaxies, the diffuse phase, exposed to the diluted radiation of all the stars in the galaxy. Rather, the dust has to be quite close to the energy sources. For instance, if we use the models of Désert et al. (1990), which assume an optically thin line of sight from the radiation source to the grains, we can compute the maximum distance at which grains have to be from a star cluster to produce a “ $60\ \mu\text{m}$  peaker” SED. Table 9 in Désert et al. (1990) lists the SED of grains exposed to the radiation of an O5 star as a function of distance. One should be as close as  $\sim 2\ \text{pc}$  of such a star to observe a significant peak at  $60\ \mu\text{m}$ . For an SSC of 500 O5 stars, this converts to a distance of  $\sim 40\ \text{pc}$ . Given that optically visible SSCs have core-haloes structure with characteristic sizes of 3 and 30 pc (O’Connell et al. 1994), this forces the dust to be the closest possible to the SSC.

This predominance of warm dust in the IR SED and the presence of a silicate absorption band at  $10\ \mu\text{m}$  indicate that we can probably not assume that the dust is optically thin to the heating radiation. These properties also imply that the dust will have a profound impact on the spectral shape of the radiation from whatever source is heating it. In this paper, we take advantage of the fact that we have a good sampling of the infrared SED, as well as a very precise description of the optical-UV SED, to constrain and model the transfer of radiation from SSCs through the dust phase.

We used DUSTY (Ivezić & Elitzur 1997; Ivezić et al. 1999) to reproduce the SED of SBS 0335-052. The currently available version of DUSTY takes into account absorption,

emission and scattering by dust. By correctly treating the radiation transfer process, it allows for the possibility that colder dust absorbs radiation emitted by the hotter dust phases, i.e. dust self-absorption, an effect that is neglected systematically when the dust phase is simply treated as a screen (such as in Paper I). Its two main limitations are (1) that it solves the problem of radiation transport only in a spherical environment and (2) that it does not include the treatment of stochastic heating<sup>7</sup>. We will come back in section §5 on the consequences of these limitations but we already note that (1) SBS 0335-052 is located too far away for us to be able to give prescriptions on the correct geometry for the dust distribution, and (2) the SED shows no sign of UIB, which implies that a much smaller fraction of the dust phase undergoes impulsive heating than in more normal galaxies.

Finally we note that a second model exists that treats the same problem in a more general way (i.e. the DIRTY model, Gordon et al. (2001); Misselt et al. (2001)) using a Monte-Carlo approach, while DUSTY solves the problem exactly. However this model is not yet in the public domain.

For DUSTY, we just have to specify the normalized spectrum of the radiation source, i.e. the central star cluster, the dust composition mix and its radial distribution, and the code calculates the dust temperature radial distribution and the emerging radiation field. Note that DUSTY uses the self-similarities included in the transfer problem to simplify the computation, so all the output results are dimensionless and have to be scaled back to the observed SED (see section §4).

### 3.2. Input parameters for DUSTY

As the input radiation, we used the spectrum from a 5 Myr old starburst calculated by Starburst99 (Leitherer et al. 1999) with a [1-100]  $M_{\odot}$  mass range. The effect of the burst age (from 3 to 25 Myr) on the emerging SED is negligible once the optical depth is sufficiently high, hence the age of the central starburst is unconstrained by the fit. This particular choice of burst age is motivated by the NIR analysis of Vanzi et al. (2000), and we come back to this in section §5.2. Note that the stellar mass we deduce in this section is dependent not only on the age of the cluster, but also on the stellar mass range. Inclusion of lower-mass stars, though not noticeable in the SED and luminosity of the source, leads to a higher total

---

<sup>7</sup>When the internal energy of a grain becomes small compared to that of a single photon, each absorption produces a spike in the grain temperature, followed by cooling. The grain never reaches thermal equilibrium and its temperature history reflects the absorption of each photon. In a given radiation field, it is always the smaller end of the size distribution that will undergo stochastic heating.

stellar mass.

Most of the free parameters of the model reside in the description of the dust located around the source. They are (1) the dust chemical composition, (2) the temperature at the inner edge of the dust shell, (3) the dust grain size distribution, (4) the normalized density law along the shell radius, and (5) the optical depth through the full dust cocoon.

The dust composition can be chosen from a variety of grain types, but we decided to stick with the commonly used composition (Weingartner & Draine 2001): silicate and graphite from Draine & Lee (1984), and amorphous carbon from Hanner (1988). The relative proportion of each of the component is a free parameter. The chemical mixture of the grains is more easily constrained when we have a detailed spectrum, but we can still assess the presence or absence of a grain type from the broad-band SED. To exemplify how each dust component leaves its mark on the output SED, Figure 2 shows the behavior of the SED for dust composed of a single element. Obviously the depth of the absorption at  $9.8\ \mu\text{m}$  is very sensitive to the relative proportion of silicate. In the absence of silicate, graphite will be responsible for most of the emission below  $9\ \mu\text{m}$ , while amorphous carbon will mostly fill the range between  $20$  and  $100\ \mu\text{m}$ .

The separation between the dust shell’s inner face and the radiation source is prescribed by the dust temperature at the inner radius  $T_1$ . This is in fact the only parameter of DUSTY that has a dimension. Thermal equilibrium of dust at the inner radius links the temperature, the central cluster SED and the inner radius. Since the cluster SED is normalized, choosing  $T_1$  selects the inner radius  $r_1$ .

The grain size distribution, based on an MRN-type (Mathis et al. 1977) distribution,  $n(a) \propto a^{-q}$  for  $a_{min} \leq a \leq a_{max}$ , is very critical, as it affects strongly the shape of the SED: the larger number of smaller grains there are, the more flux we observe in the  $8\ \mu\text{m}$  region. The lower and upper cut-off have the same practical effect as  $q$ .

The dust distribution is spherical and has a radial density dependence that we choose to follow a broken power-law  $\eta \propto y^{-\beta}$ , where  $y$  is the radial position normalized to the inner radius of the dust shell  $r_1$ . In DUSTY the dust extends from  $y = 1$  to  $y = 1000$ . The position of the breaking points as well as  $\beta$  are difficult to constrain, as we do not know for sure the matter distribution in a SSC, nor that which should be present in the cloud(s) where SSCs form. We separated the shell in three zones, from  $r_1$  to  $10r_1$ , from  $10r_1$  to  $100r_1$  and from  $100r_1$  to  $1000r_1$ , with each of them having its own radial dependency  $\beta$ . This separation is not completely arbitrary. It is first done because no acceptable fit of the observed SED was possible with a single dust zone. Then it is introduced to allow some flexibility on the radial dependance of the dust density, and also to understand the effects of the radial density on

the emerging spectrum. In Figure 3 we show some of the effects that a change in  $\beta$  in the different zones has on the emerging SED. For instance, with a rapid drop of density in the first zone ( $\beta = 2$  or  $3$ ), more dust can be heated to high temperature, giving a rise in the flux at short MIR wavelengths. On the opposite, flatter density profiles shift the SED toward longer wavelengths as more dust is far away from the heating source.

Finally, the optical depth is the most important parameter, since it critically determines how much dust is needed to produce the observed SED.

To summarize, the free parameters in the model are the optical depth  $\tau$ , the dust inner shell temperature  $T_1$ , the exponents  $\beta$  for the three density zones, the relative proportions of each dust components, and the parameters of the dust size distribution,  $a_{min}$ ,  $a_{max}$ , and  $q$ . This rather large number of parameters is constrained by 9 broad-band values of flux and the ISOCAM spectrum, which provides 25 additional independent measurements. Hence the fit is over-constrained.

#### 4. Results from the model

The best model fitting the SED of SBS 0335-052 is presented in Figure 1 and the parameters used ( $\tau$ ,  $T_1$ ,  $\beta(r)$ ,  $a_{min}$ ,  $a_{max}$ ,  $q$  and dust chemical composition) are given in Table 2. Comparison of a DUSTY SED with the observed one is made by convolving the model SED with each filter’s bandpass. We choose not to deredden the observed SED from the effect of foreground Galactic dust as the amplitude of this correction is negligible from the MIR upward (Rieke & Lebofsky 1985). A  $\chi$ -square procedure is used to determine the best model. This model reproduces all the photometric points we have obtained for SBS 0335-052 except one, which is our own very uncertain  $10.8\ \mu\text{m}$  Gemini measurement, and falls neatly within the ISOCAM spectrum uncertainty. The most salient result of this model is that the SED requires a fairly high optical depth ( $\tau = 30$ ), higher than derived in Paper I, and obviously much higher than derived by Dale et al. (2001) or Izotov et al. (1997). We will come back to that result in section §5.

Exploration of the *chi*-square fit results allows for a quantification of the range of acceptable values for the model parameters. Acceptable fits are obtained when our parameters stay within the following ranges around the nominal values listed in table 2:  $\pm 5\%$  for the abundance fraction of each dust component,  $\pm 100$  K for the internal temperature  $T_1$ ,  $\pm 0.05\ \mu\text{m}$  for  $a_{min}$ , and  $\pm 2$  on the optical depth. The density distribution of the inner zone is very well constrained by the observed SED as the wavelength range we sample is well adapted to the temperature range in that region. The outer zone is less constrained as we lack submillimeter

data. However a steeper density fall-off would not fit the SED. For the same reason, the upper size limit of the grain distribution is not well constrained. These two effects go in the same direction: the dust mass could be increased by allowing larger grains or a shallower density profile in the outer zone.

As we will see later, a critical information that can be deduced from the fit is the size of the inner cavity where the radiation source of DUSTY resides ( $r_1$ ). The ranges quoted above allow for a 10% variation in the size of this cavity.

From the best fit model, a number of important physical parameters can be derived, which have their importance in the context of star-formation in low-metallicity objects. Among them the most important ones are the bolometric luminosity of the enshrouded source, and the total dust mass implied by the spectrum. One must remember that DUSTY is a scale-free modelling of the radiation transfer problem, thus a number of arithmetic steps are needed to derive absolute quantities such as a mass and a luminosity. Along these steps the distance to SBS 0335-052 will have to be used, which introduces another source of uncertainty in all our deductions (see below).

#### 4.1. Parameters of the central starburst

The absolute bolometric luminosity of the central source is the simplest parameter to derive from the model: the global scaling factor used to match the DUSTY SED to the observed one allows to integrate the complete IR-submm SED. This results in a central stellar luminosity of  $3.8 \times 10^9 L_\odot$ . With the assumptions that the central source is a 5 Myr old starburst described by Starburst99, this translates into  $2 \times 10^6 M_\odot$  of stars. This compares well with the value of  $6.6 \times 10^6 M_\odot$  obtained by Hunt, Vanzi, & Thuan (2001) based on Br $\alpha$  observations and an obscuration of 15 visual magnitudes. Since any acceptable fit requires a relatively high optical depth, implying that the input radiation is completely reprocessed by dust, there is a large range of acceptable burst ages and IMFs for the central sources. The only parameter of the central cluster which is well constrained is its bolometric luminosity. One should note however that since dust is more efficient in absorbing UV light, the emerging SED also constrains the input SED, but to a lesser extent.

#### 4.2. Determination of the total dust mass

Obtaining the total dust mass implied by the model is less straightforward. Basically we need to integrate the dust density over the spherical shell. This means recovering the actual

physical dimensions of  $r$  and  $\rho$  which are both normalized in DUSTY. First we derive  $r_1$ , which is the inner radius of the shell.  $r_1$  is related to the temperature  $T_1$ , and the absolute luminosity, both of which are known. In fact DUSTY provides a computation of  $r_1$  for a  $10^4 L_\odot$  luminosity; a simple scaling to the actual luminosity derived above provides  $r_1 = 0.11$  pc, with an uncertainty of  $\pm 10\%$  due to the range of models that provide an acceptable fit to the SED (see above). Since the shell extends to  $1000r_1$  the physical dimension of the system is 110 pc (but note that the observable size will depend on the selected wavelength). We will come back to the meaning of these physical dimensions, and in particular to their comparison with observed sizes for the SSCs or globular clusters in other galaxies in section §5. The outer size derived above falls below the spatial resolution in the Q-band (diffraction-limited resolution of 173 pc), and is slightly above that in the N-band (diffraction-limited resolution of 90 pc).

Recovering the absolute value of the dust density is more complicated because both the grain size distribution and the radial dependence of the density are normalized. To derive these two normalization factors, we use the fact that they are involved as well in the determination of the optical depth and can be condensed both in the  $\tau$  and the dust mass equation into a single constant  $C$ . We have the following relation between  $\tau$  and  $C$ :

$$\tau = C \int_{r_1}^{r_{max}} \sum_i p(i) \int_{a_{min}}^{a_{max}} Q_{eff}^i(a) \pi a^2 a^{-2.5} \rho(r) dr da \quad (1)$$

where  $Q_{eff}^i$  is the effective scattering and absorbing coefficient for dust component  $i$  (here silicate, graphite and amorphous carbon),  $p(i)$  is the relative proportion of each component, and  $\rho$  is the density distribution. When  $C$  is known, we get the dust mass by a simple integration over the density and the grain size distribution. Using an optical depth of 30 leads to a total dust mass of  $1.5 \times 10^5 M_\odot$ . Because of the formal similarity of the dust mass and optical depth equations, the dust mass is proportional to the optical depth as given by DUSTY.

## 5. Discussion

### 5.1. Model-dependency of the results

Before drawing conclusions about the derived properties of the embedded source in SBS 0335-052, it is worthwhile to mention how uncertain and/or model-dependent these properties are. The best constrained parameter is the bolometric luminosity, as it is already well mapped by our measurements. Next comes the stellar mass, because this is derived from the luminosity. It requires an assumption on the age, which is a priori difficult to

make (though see section §5.2). By analogy with the general star formation process, one can reason that the age of embedded sources should be smaller than the age of already visible ones. This places an upper limit at 5 Myr. The mass is then relatively well constrained since it changes only by a factor of 2 for ages between 1 and 5 Myr.

The major source of uncertainty or model-dependency is introduced by the fact that DUSTY handles only dust in thermal equilibrium. This may impact the value of the inner radius of the dust shell, as dust undergoing stochastic heating can reach higher temperature in lower radiation density environments. Given that the luminosity is well constrained, we can quantify the scale on which stochastic heating is likely to play a part. Following Désert et al. (1986) and Tran (1998), we see that grains of sizes larger than  $0.1 \mu\text{m}$  will reach thermal equilibrium for values of the inner radius  $r_1$  up to 400 pc, while grains larger than  $0.01 \mu\text{m}$  would reach thermal equilibrium for values of  $r_1$  up to 4 pc. We also find from Puget & Léger (1989) that PAHs would be destroyed by the radiation for values of the inner radius of up to 11 pc. The conclusion of this is that, at least for the first few parsecs at the base of the shell, solely on the basis of energy considerations, we can exclude both the existence of small grains, and an important contribution of stochastic heating to the thermodynamics of the system. We therefore feel confident that the assumption of the whole population of dust grains being at thermal equilibrium at the base of the shell is correct, and that the actual value of  $r_1$  is also well-constrained (but see also section 5.2).

The effect of assuming thermal equilibrium over the whole shell is harder to estimate. As radiation propagates through the shell, it is reddened and thus its ability to be absorbed by grains or destroy them is lessened. The effect of allowing smaller-sized grains which undergo thermal fluctuations is basically to have a higher emission at short wavelengths per unit mass. It is thus likely that a model allowing thermal fluctuations would require less mass than DUSTY. Yet most of the mass is actually provided by the colder dust producing the long-wavelength emission and for which the assumption of thermal equilibrium is correct, therefore the correction due to thermal fluctuations on the dust mass is likely small.

To be able to more accurately represent the situation in SBS 0335-052, a model would actually require not only that thermal fluctuations be allowed but also that the size distribution change with radius. No such model is currently available.

## 5.2. The embedded star cluster

The stellar sources still embedded in their dust and molecular gas cocoons cannot be described with precision from direct observations, as they are invisible in the UV and NIR

range. The only way to get to their fundamental parameters is again by looking at the SED produced by DUSTY with the assumed starburst spectrum. We used a 5 Myr population starburst, as proposed by Vanzi et al. (2000), with a Salpeter IMF between 1 and  $100M_{\odot}$ . It should be noted that given the optical depth, the origin of the NIR emission collected by Vanzi et al. (2000) is probably composite. Our model shows that only a fraction of  $< 10^{-3}$  of the stellar luminosity emerges shortward of  $3\mu\text{m}$ . However the extinction in the K-band is only  $\sim 3$  mag, which means that emission lines produced in the gas surrounding the cluster could be observable. The age deduced by Vanzi et al. (2000) comes mainly from broad-band colors, but, as stated by the authors, these are highly contaminated by nebular emission. Therefore it is likely that this age is indeed representative of the actual age of the stellar cluster. Furthermore, if what we observe is a still embedded star-formation site, we can adopt the age measured in the NIR, since it should represent an upper limit to the age of the embedded sources. The total stellar mass thus inferred,  $2 \times 10^6 M_{\odot}$ , is only a lower limit (more mass is required for an older cluster to achieve the same luminosity). The bolometric luminosity, at  $3.8 \times 10^9 L_{\odot}$ , is much better constrained, as it comes directly from the SED. How does this source compare with other embedded or optically visible SSCs, or with globular clusters?

Though little statistics exists on the properties of SSCs, the derived mass of the SBS 0335-052 stellar source is rather typical. For instance, Smith & Gallagher (2001) get masses of  $0.5\text{--}1.2 \times 10^6 M_{\odot}$  for SSCs in NGC 1705, NGC 1569 and M82. The embedded SSC in the Antennae has a mass of  $1.6 \times 10^7 M_{\odot}$  (Gilbert et al. 2000), while Mengel et al. (2002) measure masses in the range  $0.65\text{--}4.6 \times 10^6 M_{\odot}$  for five young visible clusters in the same galaxy. The mass we derive is also similar to that of the brightest MIR cluster seen by Vacca et al. (2002) in He 2-10.

Luminosity-wise, the SBS 0335-052 source is remarkably similar to the radio super nebula in NGC 5253 (Gorjian et al. 2001), which requires  $0.8\text{--}1.2 \times 10^9 L_{\odot}$  to produce its observed radio flux. Therefore, even if such a luminosity is extreme for a single SSC, it is not the only object of its kind.

The fact that we observe this source in a chemically young object as well as in more evolved galaxies is very interesting as it points toward a common phenomenon for violent star formation, regardless of metallicity.

A further advantage of having performed a model of the radiation transfer in the object is that we now have access to intrinsic scale lengths of the cluster. To follow the geometry used by DUSTY, all of the stars have to be inside  $r_1 = 0.11$  pc. This is remarkably compact. The compact size leads to a very large stellar density of  $3.8 \times 10^8 M_{\odot} \text{pc}^{-3}$ . It is difficult to compare that density with that of other SSCs as these are rarely resolved. We note that it

is much higher than that of globular clusters (for instance the peak stellar density of M 15 is  $1.6 \times 10^6 \text{ M}_\odot \text{ pc}^{-3}$  (Meylan et al. 1997), while the mean stellar density of M 80 inside its core radius of 0.3 pc is  $3.3 \times 10^5 \text{ M}_\odot \text{ pc}^{-3}$  (Madore 1980), approximately identical to that of the young galactic center Arches cluster (Serabyn et al. 1998)). It is impossible to know whether the very high stellar density we derive is a problem as few models deal with the formation of SSCs. We note however that such a compact cluster would have an uncomfortably large virial velocity dispersion (of the order of  $300 \text{ km.s}^{-1}$ , much larger than any observed velocity dispersions in SSCs, e.g. Mengel et al. (2002)), leading to a very small dynamical time (of the order of a few hundred years).

This situation can be relaxed if the radius of the volume actually occupied by stars is allowed to grow to 1 pc. Indeed, with this value, the stellar properties of the SSC would become absolutely average compared to SSCs and globular clusters. As mentioned in section 5.1, this could be feasible by allowing thermal fluctuations in the model. With this, the inner radius could be increased by the fact that temperatures higher than those derived from the thermal equilibrium equation could occur further from the center. We note however that it is the smaller sized grains that can run into that regime, and that they are also thought to be less resilient to destruction by radiation.

A more realistic possibility to allow the volume occupied by stars to grow beyond the one attributed by DUSTY is to consider that, contrary to the situation assumed by the model where dust and stars are segregated, they are mixed in an inner region. Such a situation cannot be computed with DUSTY, but it is likely that it would make little difference in the principal outputs of the model. First, it is true that by allowing the stellar cluster to expand, we lower the mean radiation density in the inner region of the system. This may lead to a decrease of the dust temperature, and thus of the MIR emission, which can be compensated either by thermal fluctuations mentioned above, or by allowing grains to get closer to the radiation sources. Thus the hot dust required to produce the MIR emission in the inner part of the system (so that it is later absorbed) can still be present in this “mixed” geometry. With an expanded cluster and dust mixed with it, we also decrease to total optical depth. However, with the density profile of the structure (see table 2), most of the dust, and thus of the optical depth, is located in the outer parts of the structure, and will not be impacted by the changes occurring in the inner parts. This kind of geometry can unfortunately not be explored by DUSTY since having an extended radiation source breaks one of the requirements to exploit the self-similarities in the radiation transfer problem. We however feel confident that such a situation would keep most of the important outputs of the model.

To be complete, we should also state that the distance to SBS 0335-052 is involved in

the determination of the stellar density to a power of -2.5 to -2.3 (depending on the actual mass to light ratio of the cluster stars). This is a strong dependency. However to obtain more standard values of the stellar density would require unrealistically large errors on the distance determination.

Finally we want to emphasize again that the dust cocoon, as we model it, is extremely efficient at blocking the light of the stars: less than  $10^{-3}$  of the bolometric luminosity emerges shortward of  $3\ \mu\text{m}$ . With a high enough spatial resolving power, this would lead to exactly the same situation as observed in He2-10 where the visible up to K-band morphologies are very similar, but completely different from the MIR morphology (Vacca et al. 2002).

### 5.3. The dust properties in SBS 0335-052

The first interesting point of our experiments with DUSTY is that a pure silicate dust phase is ruled out, contrary to what was suggested in Paper I. The dust chemical and size composition is very well constrained by the Gemini Q-band observation and by the ISOCAM spectra. The strong continuum of the ISOCAM spectra as well as the relative shallowness of the two silicate bands are highly indicative of an important contribution to the emission by graphite and amorphous carbon, both carbon-based (see Figure 2) even though no PAH signatures are visible in the spectrum. The absence of the PAH bands is thus not a strong argument in favor of the absence of any carbon-based dust.

That the galaxy may be undergoing one of its first burst of star formation is not an argument against carbon-based dust either since carbon dust is rapidly formed in the ejecta of supernova (Todini & Ferrara 2001), which may have already exploded in other regions of the galaxy, as indicated by the shell-like structures observed by Thuan et al. (1997).

The size distribution that we observe is also very interesting as it is quite different from the standard MRN distribution, both in the range of grain sizes allowed and in the exponent of the distribution (see Table 2). Yet this size distribution is not completely new as it is very similar to that deduced from extinction studies around the central engine of AGNs. For instance, Maiolino et al. (2001) showed that the size distribution that explains best the extinction observed toward AGNs is depleted in small grains, has a rather high maximum size ( $\sim 1\ \mu\text{m}$ ), and follows a power law with an exponent of  $-2.5$ , as found for the best-fitting model for SBS 0335-052. This obviously does not imply that we have a mini-AGN at the heart of SBS 0335-052, and in fact all spectroscopic data show that the source is powered

by star formation<sup>8</sup> (see e.g. Vanzani et al. (2000)). It is however quite consistent with model-independent considerations on the energetics of the heating source: indeed if we express the mean energy density as a function of  $y = r/r_1$ , neglecting for the moment the presence of the dust, we obtain that  $\rho_E(y) = 2.1 \times 10^5 y^{-2} \text{ eV cm}^{-2}$ . This means that at the base of the dust shell, the energy density is 4 orders of magnitude higher than the value that would allow PAHs, *i.e.* the smallest dust grains, to survive (Puget & Léger 1989).

The fact that the model tends to exclude small grains also indicates that we are dealing with a very young star-forming region. Indeed, shocks such as those generated by supernovae are very efficient in destroying the large grains to replenish the smallest sizes (see e.g. Jones et al. (1996)). A dust size distribution biased toward the large grains suggests on the contrary that most of the dust is still as it was when large molecular clouds condensed to form a proto-SSC and that no significant sweeping by SN shocks has yet occurred (dust sizes are known to grow in dense environments, see e.g. Maiolino (2002)).

This exclusion of small grains, both on the basis of the model and on that of the energy content of the source also brings further support to the choice of DUSTY to model the radiative transfer. As indicated in section 3, DUSTY only treats grain in radiative equilibrium. For any given radiation density level, the smallest dust grains will not reach thermal equilibrium but rather undergo thermal spiking, reaching temperatures much higher than the theoretical equilibrium ones (Tran 1998). The size threshold to switch from thermal equilibrium to thermal spiking is a decreasing function of the energy density. Here we have both a very high energy density, at least in the inner part of the dust shell, and a high minimum size for the dust grain. These two properties go in the same direction which is to limit the importance of thermal spiking with respect to thermal equilibrium.

Regarding the radial dependence of the dust density, we note that it is impossible to reproduce the full SED of SBS 0335-052 *and* the ISOCAM spectrum with a steeper distribution than what we used. This would lead to an overproduction of luminosity in the  $10 \mu\text{m}$  region. This emission can be compensated by a higher optical depth, but this would cause a too strong silicate absorption band at  $9.7 \mu\text{m}$ . The last region of the density distribution, from  $100r_1$  to  $1000r_1$ , is mainly affecting the longer wavelength SED, as it contains mostly rather cold dust. It affects strongly the dust mass, being colder and distributed over a large region, as it is the case for all galaxies. The  $60 \mu\text{m}$  PHT observation constrains the external part of the distribution: too steep a distribution does not produce enough luminosity at this wavelength.

---

<sup>8</sup>From our modelled SED we synthesized the fluxes required for the diagnostic diagram of Laurent et al. (2000). These showed that SBS 0335-052 is placed far away from the AGN region of the diagram.

As an aside, our fitted SED predicts fluxes of  $0.55 \mu\text{Jy}$  and  $0.03 \mu\text{Jy}$  respectively at  $450 \mu\text{m}$  and  $850 \mu\text{m}$ , a range of fluxes that are unfortunately not accessible to current sub-millimeter telescopes.

#### 5.4. The optical depth and dust mass

The most important result of this paper is that we confirm, on a much more solid basis, the high optical depth of the dust cloud measured in Paper I. The reason for the difference between the value of 21 V mag quoted in Paper I and the present result of  $\sim 30$  resides in the fact that Paper I used the unrealistic assumption of a screen of dust, while here we account more correctly for the transfer of radiation through the dust. Our result is thus completely at odds with that of Dale et al. (2001) that argued for an optically thin source. Let us examine the reasons for this discrepancy. The choice of a model that is able to solve radiation transfer obviously does not bias the result toward high optical depths, as DUSTY is perfectly able to reproduce optically thin SEDs. On the opposite, Dale et al. (2001) follow a number of questionable steps to arrive at the result that  $A_V \simeq 1$ : they derive their optical depth using the link between the optical depth and the surface brightness of a blackbody emission. While this relation is exact, they still need to represent the SED as a sum of blackbodies, and have a measure of the size of the emitting region. Rather than attempting to model the SED on a physical basis, they simply fitted the SED with two blackbodies. We note that somewhat arbitrarily large error bars were added to the measurements presented in Paper I and that the resulting SED shows quite a poor match with the ISOCAM spectrum of Paper I. Regarding the size of the emitting region, they have assumed that the emission is uniform over the size of the object, as resolved by their observation ( $80 \pm 5 \text{ pc}$  FWHM). This is possibly the most questionable step of the reasoning as the deduced value of  $A_V$  is proportional to this surface. Our computation of the radiative transfer shows that even if the dust shell extends up to  $100 \text{ pc}$ , its FWHM *as observed in the N-Band* is much more compact, probably less than  $1 \text{ pc}$ . Even if the inner radius of the shell was increased by thermal fluctuation (see section 5.2), we do not expect that the emission would have a constant surface brightness, but rather show a core-halo structure that invalidates the use of the full size of the emitting region in the computation of  $A_V$  by Dale et al. (2001).

The dust mass derived using DUSTY is of  $1.5 \times 10^5 M_\odot$ . This is very close to the estimate of Hunt, Vanzi, & Thuan (2001) using an independent method, and inside the interval determined in Paper I. Not surprisingly it is much more than the estimate of Dale et al. (2001), because the incorrect assumptions on the SED and on the object size propagate in the dust mass computation. Although this is a small intrinsic quantity with respect to

the  $9.5 \times 10^8 M_{\odot}$  of HI present around the galaxy (Thuan et al. 1999a), this is rather large for such a metal-deficient object. Does the star formation history of SBS 0335-052 allow for the formation of this dust phase? In young starbursts, most of the dust is provided by type-II supernovae (SNe II). Hirashita et al. (2002) have studied the problem of dust formation in low-metallicity environments, such as SBS 0335-052. Their work shows that the dust mass we measure can be accumulated in approximately  $5 \times 10^7$  yr of continuous star formation at a rate of  $1 M_{\odot} \cdot \text{yr}^{-1}$ . Papaderos et al. (1998) showed from broad-band colors that the brightest visible clusters have ages in the range  $0.1\text{-}3 \times 10^7$  yr, while another set of  $\sim 10$  fainter clusters have ages in the range  $3\text{-}10 \times 10^7$  yr. Therefore the amount of dust we measure is nearly consistent with the idea that the dust was produced in the recent star-formation sites currently observed in the visible. We note that in the context of a continuous star-formation scenario such as proposed by Legrand et al. (2000) for I Zw 18, we would have much more time to build up the dust phase. However in that case we would have (1) to take into account destruction processes that are neglected in Hirashita et al. (2002), and (2) make sure that dust which has been exposed to supernovae shock waves has enough time to coagulate so that we observed the biased size-distribution required by the SED.

### 5.5. The lifetime of an embedded SSC

The question of the lifetime of an embedded SSC such as the one in SBS 0335-052 is an important one, as it has a heavy bearing on our ability to correctly account for all star formation activity in a galaxy. Dust in the envelope of the SSC is subject to three main forces from the SSC: radiation pressure and impact from stellar winds will blow the dust out, while gravitation will attract it inward. Following Weingartner & Draine (2001) and Tenorio-Tagle & Medina-Tanco (1998) we can express the sum of the radiation pressure and impact from stellar winds as:

$$P_{rad+wind}(a) = \frac{1}{4\pi r^2} \left[ \frac{\langle Q_{pr}(a) \rangle L_{\star}}{c} + \dot{M}_{wind} v_{wind} \right], \quad (2)$$

where  $L_{\star}$  is the bolometric stellar luminosity,  $\langle Q_{pr}(a) \rangle$  is the luminosity averaged radiation pressure efficiency on a grain of size  $a$ ,  $\dot{M}_{wind}$  is the cluster's wind mass-loss rate,  $v_{wind}$  is the wind terminal velocity. From Starburst99, we obtain the kinetic luminosity ( $\dot{M}_{wind} v_{wind}^2 / 2$ ) of the cluster,  $5.2 \cdot 10^6 L_{\odot}$ . We can therefore express the ratio of the radiation and kinetic pressure as:

$$P_{rad}/P_{wind} = 9.7 \cdot 10^{-7} v_{wind} \langle Q_{pr}(a) \rangle. \quad (3)$$

Thus assuming a wind terminal velocity of  $10^6 \text{ m}\cdot\text{s}^{-1}$ , typical of main-sequence O stars, we obtain that the two terms are of the same order of magnitude at the base of the dust

shell where  $\langle Q_{pr}(a) \rangle$  is 1-2. Weingartner & Draine (2001) showed that under anisotropic radiation, photoelectron emission and photodesorption of molecules from grains can act as an added pressure, in some cases increasing the radiation pressure efficiency by a factor of 20. In that case, radiation effects will dominate. As a side note, let us mention that the observed linewidths of only 160-170 km.s<sup>-1</sup>, as observed for instance by Turner et al. (2001) toward the radio supernebula in NGC 5253, are not incompatible with the value chosen here for the wind terminal velocity. Indeed, what is measured is the outflow of ionized gas (through the velocity broadening of the nebular Br $\gamma$  emission line), which is coupled with the molecular and dusty envelope of the SSC and hence slowed down by wind momentum conservation.

How then does radiation pressure compare to gravity? Laor & Draine (1993) express the ratio of the acceleration produced by these two forces in the optically thin case as:

$$\Gamma(a) = \frac{g_{rad}}{g_{grav}} = \frac{3L_{\star} \langle Q_{pr}(a) \rangle}{16\pi ca\rho GM_{\star}}, \quad (4)$$

where  $M_{\star}$  is the mass of the stellar cluster, and  $\rho$  the density of the dust grain. This optically thin case applies well to the base of the dust shell and, using  $\rho = 3 \cdot 10^3$  kg.m<sup>-3</sup>, this gives numerically  $\Gamma(a) = 360 \langle Q_{pr}(a) \rangle / a_{\mu m}$ . We thus see that radiation pressure overtakes gravity by several orders of magnitude at the base of the shell, i.e. that it can be moving the shell outward. At the outer boundary of the shell the situation may be different since there, the luminosity is heavily reddened and therefore the luminosity-averaged radiation pressure efficiency will be much lower. Using the formula for  $\Gamma(a)$  given by Laor & Draine (1993) in the optically thick case, we see that in the outer parts of the shell, gravity and radiation pressure almost balance each other ( $\Gamma(a) \simeq 1.7$ ). It is unlikely that the effects described in Weingartner & Draine (2001) will occur at the outer boundary of the shell since the radiation is now too soft to allow photoelectron emission or photodesorption of molecules to occur.

Since this neglects the influence of an outer pressure, we have here an indication that an embedded SSC may be a long-lived structure, lasting at least till the first supernovae explode. This is however only indicative. Indeed, a simple calculation of the motion of a grain subject to radiation pressure, stellar winds and gravity from an SSC such as the one we deduce in SBS 0335-052 shows that it can be quite efficiently blown away from the SSC. Timescales derived from such a calculation are however incorrect since grains will feel a strong drag from collisions with the gas that is associated to them. This drag will probably be even stronger at the base of the shell where ionization of gas and grains can lead to a very efficient coupling of the two phases (Ferland 2001). A detailed modelling of the dynamics of such a region would therefore be a worthwhile endeavor in order to constrain the lifetime of the SSC embedded stage. We note that the presence of similar objects in a number of sources (e.g. He 2-10, NGC 5253, NGC 4038/9) indicates that these lifetimes cannot be extremely

short. On the other hand, the fact that the age of optically visible clusters are in the range of a few Myr probably sets an upper limit to the embedded stage lifetime.

### 5.6. Implications for star-formation at high redshift

SBS 0335-052, with an extremely low metallicity, is already a galaxy where much of the star-formation activity is completely hidden from view from UV to NIR, possibly for a significant fraction of the starburst lifetime. The  $3.8 \times 10^9 L_{\odot}$  bolometric luminosity of the cluster translates into  $3.8 \times 10^4$  equivalent O7 stars. This is a factor of 10 more than the number of equivalent O7 stars required to power the visible clusters (Hunt, Vanzì, & Thuan 2001). This demonstrates that even in extremely low-metallicity objects, the visible-UV part of the SED may be relatively insignificant and is not a reliable indicator of the actual star-formation activity. In this respect, SBS 0335-052 can be considered as a smaller and nearer analog to the  $z = 2.56$  submillimeter galaxy SMM J14011+0252 studied by Ivison et al. (2001). Therefore it could very well be that most of the star-formation episodes that occur during the first phases of galaxy formation are completely hidden from view in the short wavelength part of the electromagnetic spectrum. We already see that the embedded SSC phenomenon happens in numerous dwarf galaxies, irrespective of their metallicity. Therefore it only remains to be seen whether the process of star formation, as we observe it in dwarf galaxies, provides a suitable analog to the situation occurring in primeval objects.

## 6. Conclusion

We have modelled the infrared SED of the blue compact dwarf galaxy SBS 0335-052 with DUSTY, which solves consistently the radiation transfer in a spherical distribution of dust. From this modelling, we deduce that SBS 0335-052 harbors a deeply embedded super-star cluster, effectively hidden under about 30 mag of visual extinction. The low-metallicity of the galactic gas did not preclude the formation of the  $10^5 M_{\odot}$  of dust necessary to completely hide from the optical view the SSC. With  $2 \times 10^6 M_{\odot}$  of stars and an age of probably less than 5 Myr, the SSC has not been able yet to pierce through the cocoon of dust and gas from which it formed, but it had a profound effect on the dust size distribution: the hardness of the radiation destroyed the smallest dust particles and the PAH but shocks did not alter yet the larger size grains up to  $1 \mu\text{m}$ . The standard MRN distribution, normally observed in quiescent galactic environment, cannot reproduce the IR data we have at hand. Instead, the dust in the SSC environment is reminiscent of what we observe around AGN, emphasizing the role of density and radiation hardness on the dust grain size distribution. If dust-enshrouded

SSCs are commonly associated to starbursting environment, the star-formation rate deduced by looking at the rest-frame optical or UV should be taken with caution. Even with IR or MIR information care should be taken to use a correct radiation transfer treatment and one should use an extinction law suited to the radiation and gas density of the observed source.

We warmly thank Martin Haas of the ISOPHT data center in Heidelberg and Scott Fisher of Gemini North for assistance and advice in the data reduction. Jean-Luc Starck's guidance on the use of wavelet analysis was deeply appreciated. Many thanks to Carmelle Robert, Jean-René Roy and Pierre-Alain Duc for helpful discussions and comments on the manuscript. We also acknowledge the critical reading of our anonymous referee that led us to a more in-depth analysis of important parts of this paper, resulting in, we hope, a more convincing study.

## REFERENCES

- Allamandola, L.J., Tielens, A.G.G.M., & Barker, J.R. 1985, *ApJ*, 290, L25
- Calzetti, D., Kinney, A. L., & Storchi-Bergmann, T. 1994, *ApJ*, 429, 582
- Cannon, J. M., Skillman, E. D., Garnett, D. R. & Dufour, R. J. 2002, *ApJ*, 565, 931
- Cohen, M., Walker, R. G., Carter, B., Hammersley, P., Kidger, M., & Noguchi, K. 1999, *AJ*, 117, 1864
- Contursi, A., Lequeux, J., Cesarsky, D., Boulanger, F., Rubio, M., Hanus, M., Sauvage, M., Tran, D., Bosma, A., Madden, S., & Vigroux, L. 2000, *A&A*, 362, 310
- Dale, D. A., Helou, G., Neugebauer, G., Soifer, B. T., Frayer, D. T. & Condon, J. J. 2001, *AJ*, 122, 1736
- Désert, F. X., Boulanger, F. & Puget, J. L. 1990, *A&A*, 237, 215
- Désert, F. X., Boulanger, F., & Shore, S. 1988, *A&A*, 160 285
- Doublier, V., Caulet, A., & Comte, G. 2001, *A&A*, 367, 33
- Draine, B.T., & Lee, H.M. 1984, *ApJ*, 285, 89
- Ellis, R. 1998, *Nature*, 395, A3
- Ferland, G. J. 2001, *PASP*, 113, 41

- Gilbert, A. M., Graham, J. R., McLean, I. S., Becklin, E. E., Figer, D. F., Larkin, J. E., Levenson, N. A., Teplitz, H. I. & Wilcox, M. K. 2000, *ApJ*, 533, L57
- Gordon, K. D., Misselt, K. A., Witt, A. N. & Clayton, G. C. 2001, *ApJ*, 551, 269
- Gorjian, V., Turner, J.L., & Beck, S.C. 2001, *ApJ*, 554, L29
- Hanner, M.S. 1988, *NASA Conf. Pub.*, 3004, 22
- Hartmann, L.W., Huchra, J.P., Geller, M.J., O'Brien, P., & Wilson, R. 1988, *ApJ*, 326, 101
- Heisler, C. A., & de Robertis, M. M. 1999, *AJ*, 118, 2038
- Hirashita, H., Hunt, L. K., & Ferrara, A. 2002, *MNRAS*, 330, L19
- Hunt, L.K., Vanzi, L., & Thuan, T.X. 2001, *A&A*, 377, 66
- Ivezić, Ž., Elitzur, M. 1997, *MNRAS*, 287, 799
- Ivezić, Ž., Nenkova, M., & Elitzur, M. 1999, User Manual for DUSTY, University of Kentucky Internal Report, <http://www.pa.uky.edu/moshe/dusty/>
- Iverson, R. J., Smail, I., Frayer, D. T., Kneib, J.-P., Blain, A. W. 2001, *ApJ*, 561, L45
- Izotov, Y., Lipovetsky, V. A., Chaffee, F. H., Foltz, C. B., Guseva, N.G., & Kniazev, A.Y. 1997, *ApJ*, 476, 698
- Johnson, K.E., Leitherer, C., Vacca, W.D., & Conti, P.S. 2000, *AJ*, 120, 1273
- Jones, A.P., Duley, W.W., & Williams, D.A. 1990, *QJRAS*, 31, 567
- Jones, A.P., Thielens, A.G.G.M., & Hollenback, D.J. 1996, *ApJ*, 769, 740
- Jones, A. P., d'Hendecourt, L. 2000, *A&A*, 355, 1191
- King, I.R. 1966, *AJ*, 71, 64
- Kobulnicky, H.A., & Johnson, K.E. 1999, *ApJ*, 527, 154
- Kunth, D., & Östlin, G. 2000, *A&A Rev.*, 10, 1
- Laor, A., & Draine, B. T. 1993, *ApJ*, 402, 441
- Laureijs, R. J., Klaas, U., Richards, P. J., Schultz, B., & Ábrahám, P. 2000a, *The ISO Handbook*, Vol. V. SAI-99-069/Dc, Version 1.1

- Laureijs, R. J., Watson, D., Metcalfe, L., McBreen, B., O'Halloran, B., et al. 2000b, *A&A*, 359, 900
- Laurent, O., Mirabel, I. F., Charmandaris, V., Gallais, P., Madden, S. C., Sauvage, M., Vigroux, L. & Cesarsky, C. 2000, *A&A*, 359, 887
- Léger, A., & Puget, J.L. 1984, *A&A*, 137, L5
- Legrand, F., Kunth, D., Roy, J.-R., Mas-Hesse, J. M., & Walsh, J. R. 2000, *A&A*, 355, 891
- Leitherer, C. 1999, in 'Chemical evolution from zero to high redshift', Eds. Walsh, J., Rosa M., *Lecture notes in Physics* (Berlin: Springer)
- Leitherer, C., Schaerer, D, Goldader, J.D., Delgado, R.M.G., Robert, C., Kune, D.F., de Mello, D.F., Devost, D. & Heckman, T.M. 1999, *ApJS*, 123, 3
- Lemke, D., Klaas, U., Abolins, J., Ábrahám, P., Acosta-Pulido, J. et al. 1996, *A&A*, 315, L64
- Madore B., 1980 in 'Globular clusters', Hanes, D., Madore, B (eds.) Cambridge University Press, p21
- Maiolino, R. 2002, in 'The evolution of galaxies. II. Basic building blocks', M. Sauvage et al. (eds.) in press
- Maiolino, R., Marconi, A., & Oliva, E. 2001, *A&A*, 365, 37
- Mathis, J.S., Ruml, W., & Nordsieck, K.H. 1977, *ApJ*, 217, 425
- Mengel, S., Lehnert, M. D., Thatte, N., Genzel, R. 2002, *A&A*, 383, 137
- Meylan, G., & Heggie, D. C. 1997, *A&AR*, 8, 1
- Meurer, G., Heckman, T.M., Leitherer, C., Kinney, A., Robert, C., & Garnett, D.R. 1995, *AJ*, 110, 2665
- Mirabel, F., Vigroux, L., Charmandaris, V., Sauvage, M., Gallais, P., Cesarsky, C., Madden, S. & Duc, P. A. 1998, *A&A*, 333, L1
- O'Connell, R.W., Gallagher, J. S., & Hunter, D. A. 1994, *ApJ*, 433, 65
- Misselt, K. A., Gordon, K. D., Clayton, G. C. & Wolff, M. J. 2001, *ApJ*, 551, 277
- Östlin, G. 2000, *ApJ*, 235, L99

- Östlin, G., & Kunth, D. 2001, A&A, 371, 429
- Papaderos, P., Izotov, Y. I., Fricke, K. J., Thuan, T. X., & Guseva, N. G. 1998, A&A, 338, 43.
- Pisano, D.J., Kobulnicky, H.A., Guzman, R., Gallego, J., & Bershad, M.A. 2001, AJ, 122, 1194
- Puget, J. L., & Léger, A. 1989, ARA&A, 27, 161
- Rieke, G.H., & Lebofsky, M.J. 1985, ApJ, 288, 618
- Sanders, D. B., & Mirabel, I. F. 1996, ARA&A, 34, 749
- Sauvage, M., Thuan, T. X. & Lagage, P. O. 1997, A&A, 325, 98
- Sauvage, M., et al. 2002, in preparation.
- Serabyn, E., Shupe, D. & Figer, D. F. 1998, Nature, 394, 448
- Silk, J., & Devriendt, J. 2001 in *The Extragalactic Infrared Background and its cosmological implications*, IAU Symposium, Vol. 204, M. Harwit & M. G. Hauser, eds. ASP, 423
- Smith, L. J., & Gallagher, J. S. III 2001, MNRAS, 326, 1027
- Starck, J. L., Murtagh, F., & Bijaoui, A. 1998, ‘Image processing and data analysis: the multiscale approach’, Cambridge University Press, Cambridge (GB)
- Starck, J. L., Abergel, A., Aussel, H., Sauvage, M., Gastaud, R., Claret, A., Désert, F. X., Delattre, C., & Pantin, E. 1999, A&AS, 134, 135
- Tenorio-Tagle, G., & Medina-Tanco, G. A. 1998, ApJ, 503, L171
- Todini, P., & Ferrara, A. 2001, MNRAS, 325, 726
- Thuan, T. X., Lipovetsky, V. A., Martin, J. M., & Pustilnik, S. A. 1999a, A&AS, 139, 1
- Thuan, T.X., Sauvage, M., & Madden, S. 1999b, ApJ, 516, 783
- Thuan, T.X., Izotov, Y.I., & Lipovetsky, V.A. 1997, ApJ, 477, 661
- Tran, Q. D. 1998, PhD Thesis, Université Paris XI
- Turner, J.L., Beck, S.C., & Ho, P.T.P. 2000, ApJ, 532, L109
- Turner, J. L., Crosthwaite, L. P., Meier, D. S., Beck, S. C. 2001, AAS 198, # 09.05

Vacca, W. D., Johnson, K. E. & Conti, P. S. 2002, AJ, 123, 772

Vanzi, L., Hunt, L.K., Thuan, T.X., & Izotov, Y.I. 2000, A&A, 363, 493

Weingartner, J.C., & Draine, B.T. 2001, ApJ, 548, 296

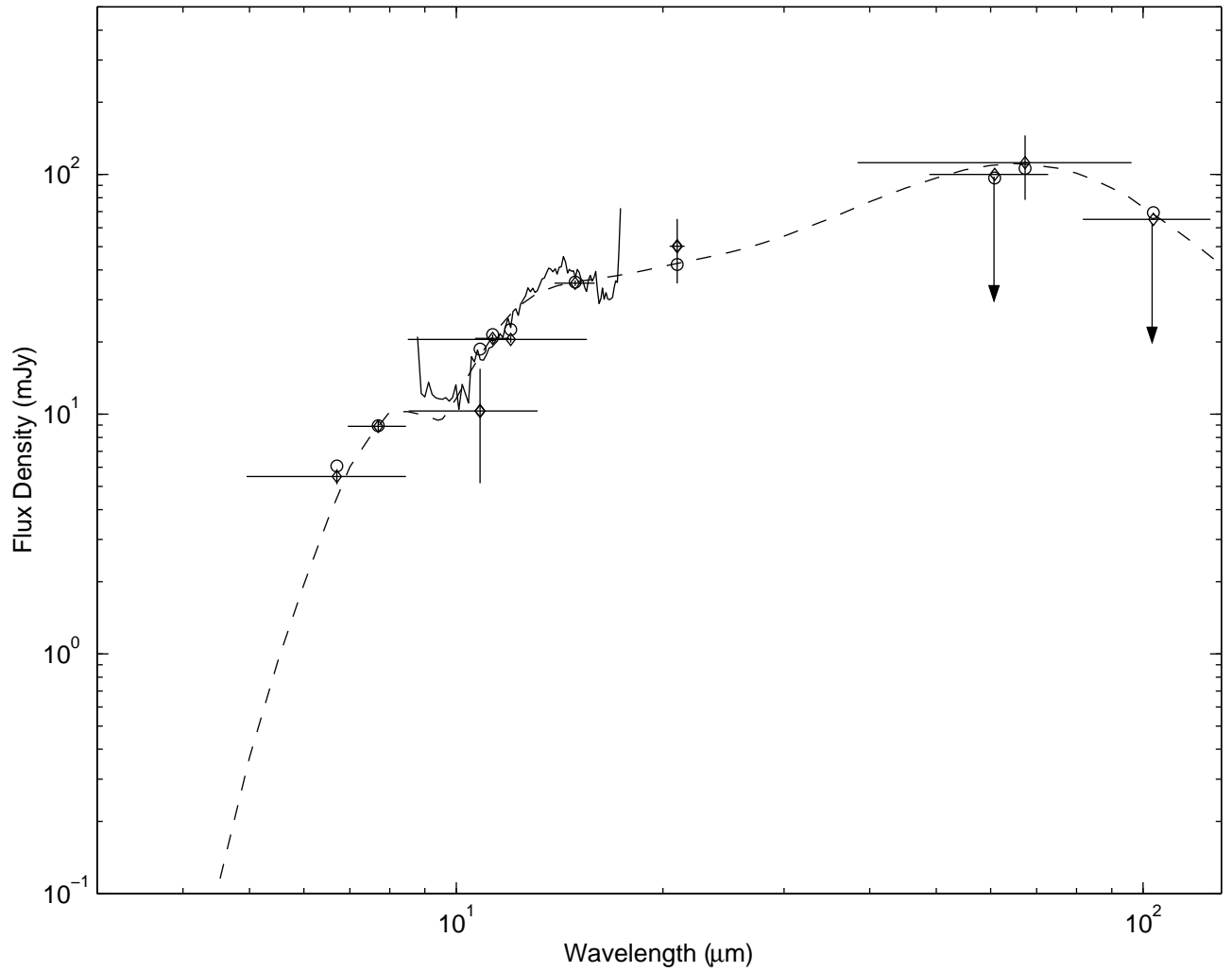


Fig. 1.— Our best DUSTY model (broken line) superposed on the SED of SBS 0335-052 (see Table 2 for its parameters). Symbols with error bars represent the observed broadband photometric data, while the solid line is the ISOCAM spectrum. Open circles represents model fluxes in the same bandpasses, synthesized from the model.

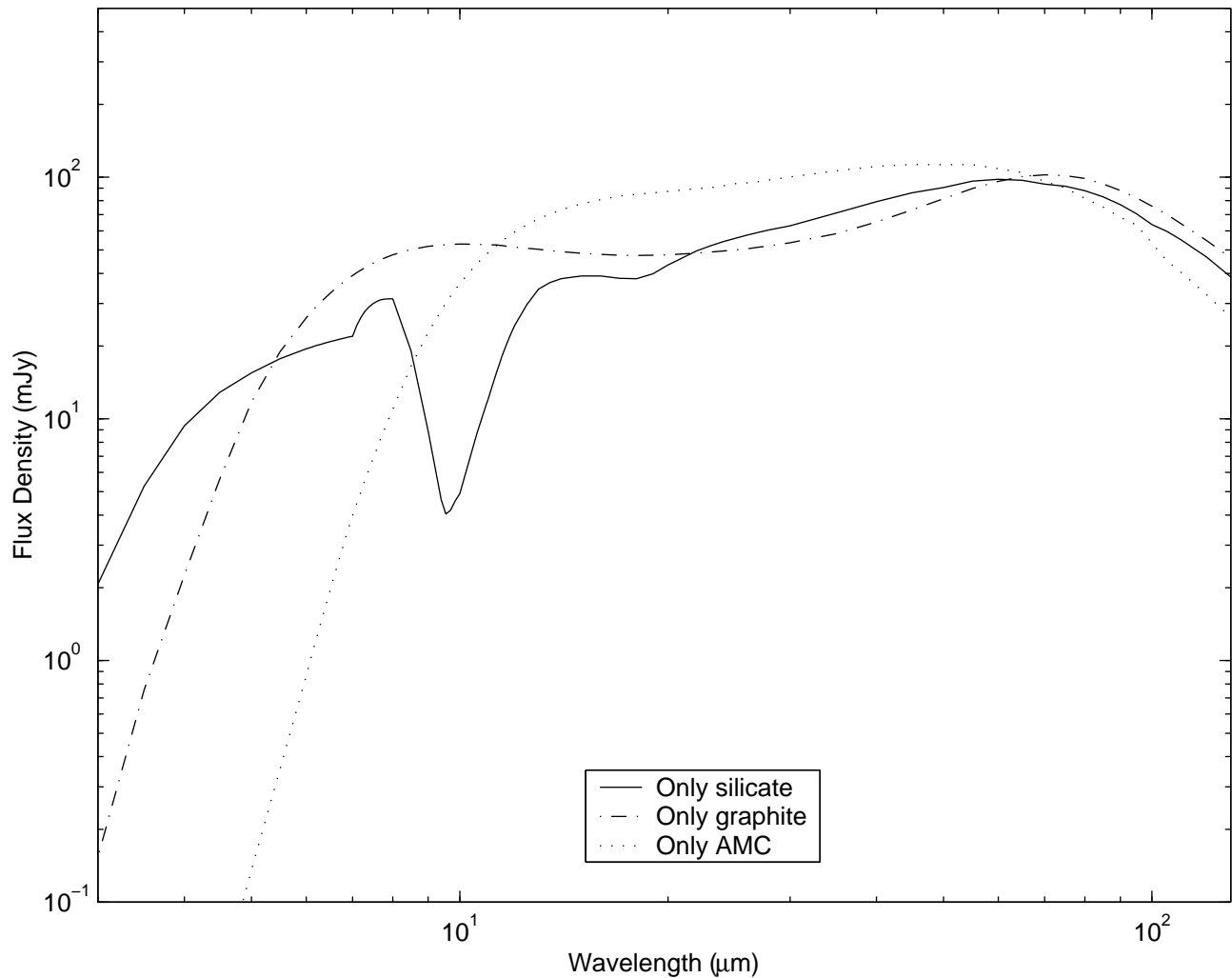


Fig. 2.— Emerging SED for pure graphite (dash-dotted line), silicates (solid line) and amorphous carbon (dotted line) dust phases, exemplifying the impact of each dust specie. The other parameters of the model are the same as those which were used to reproduce the SED of SBS 0335-052 (see Table 2).

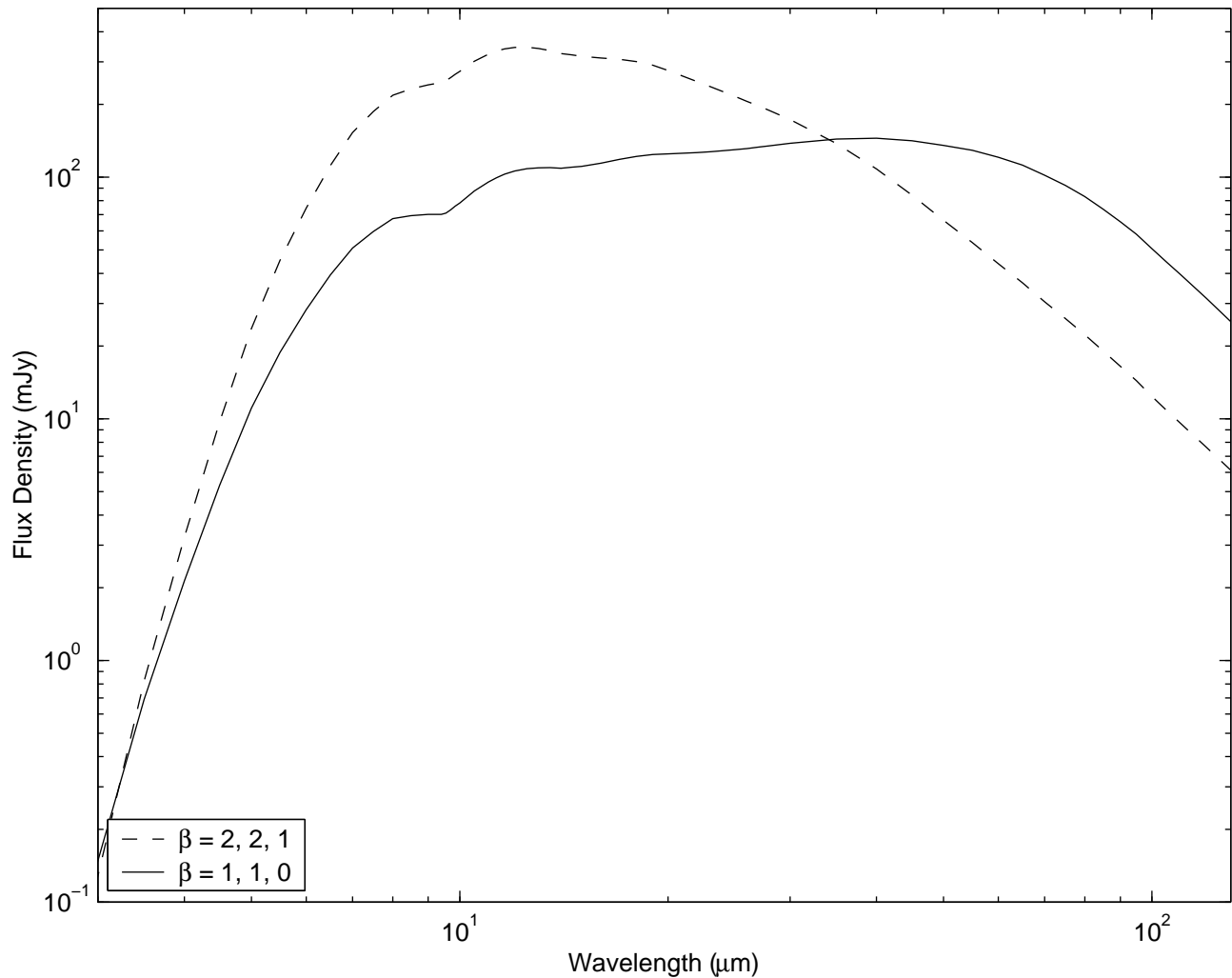


Fig. 3.— Emerging SED for different values of  $\beta$ . The breaking points of the power-law distribution are at  $r_1 = 10, 100$  and  $1000$ . The temperature (700K) and chemical composition of the grains are the same for the two distributions as those which were used to reproduce the SED of SBS 0335-052 (see Table 2).

Table 1. Photometric data used in this paper

$\lambda_{ref}$ $\mu\text{m}$	Instrument	Flux mJy	$1\sigma$ mJy
10.8	Gemini/OSCIR	10.3	50% <sup>a</sup>
21	Gemini/OSCIR	50.2	30% <sup>a</sup>
60	ISOPHOT	<100	
65	ISOPHOT	112	21
100	ISOPHOT	<65	

<sup>a</sup>These are photometric accuracies  
(see section 2.2)

Table 2. Best parameters for DUSTY to reproduce the SED of SBS 0335-052

Optical Depth at 0.55 $\mu\text{m}$		30.0
Temperature	(K)	700
Density Law ( $\beta$ )	$r_1$ to $10r_1$	1
	$10r_1$ to $100r_1$	1
	$100r_1$ to $1000r_1$	0
Elements	Silicate	23%
	Graphite	43%
	AMC	34%
Size distribution	Exponent	-2.5
	Lower cut-off ( $\mu\text{m}$ )	0.022
	Upper Cut-off ( $\mu\text{m}$ )	1